Electronic Supplementary Material (ESI) for Polymer Chemistry.

Supplementary Information

Cyclic topology effects on the morphology of biocompatible and environment-friendly poly(ε-caprolactone) under nanoscale film confinement

Li Xiang,[a] Wonyeong Ryu,[a] Jehan Kim[b] and Moonhor Ree*[a]

[a]*Department of Chemistry, Division of Advanced Materials Science, and Polymer Research Institute, Pohang University of Science and Technology, Pohang 37673, Republic of Korea*

[b]*Pohang Accelerator Laboratory, Pohang University of Science and Technology, Pohang 37673, Republic of Korea*

Synthesis

Each *c*-PCL used for structure and morphology study was prepared in a three-step manner, as shown in Scheme S1.[1]

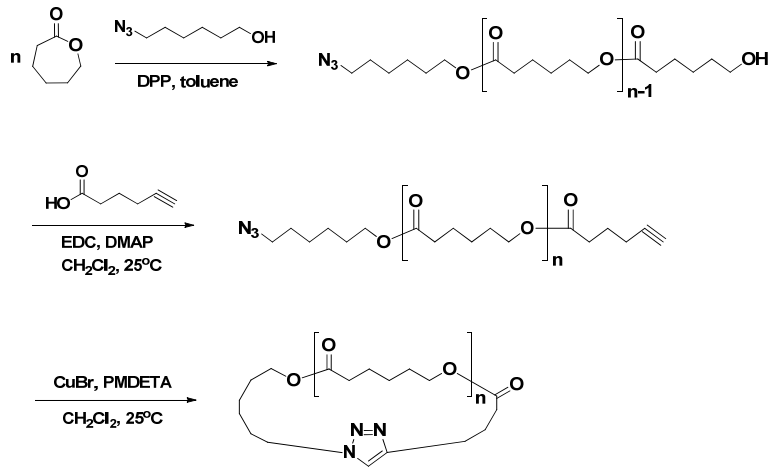

Scheme S1. Synthesis of *c*-PCL from CL: linear PCL and its cyclization via azide-alkyne click chemistry.

A representative example of synthesis is given as follows. In the first-step, a 6-azido-1-hexanol initiated polymerization of CL was conducted with [M]/[I] = 100 with the aid of diphenyl phosphate catalsy in toluene at 25 °C for 16 h in a glove box. Then, the polymerization was quenched by adding Amberlyst A21 as a small base bead for termination reaction. After 1 h, the used Amberlyst A21 was removed from the reaction mixture by filtration and the used solvent was also removed out by using a rotary evaporator with a vacuum system. The crude product was dissolved in CH_2Cl_2 and then precipitated into cold methanol, followed by filtration. The obtained product was washed with cold methanol several times and then dried at room temperature in vacuum. The α-azido-ω-hydroxy-PCL (N_3-PCL_{100}-OH) precursor product was obtained with 96.4 % yield; the product was characterized by proton (^{1}H) and carbon (^{13}C) nuclear magnetic resonance (NMR) spectroscopies; a Bruker spectrometer (model AV300 FT-NMR, Rheinstetten, BW, Germany) was employed. ^{1}H NMR (300 MHz, $CDCl_3$, δ (ppm)): 1.38 (m, 2H × n, (-$CH_2CH_2CH_2CH_2CH_2$-)$_n$), 1.57 (m, 2H × n, (−$CH_2CH_2CH_2O$−)$_n$), 1.65 (m, 2H × n, (−$COCH_2CH_2CH_2$−)$_n$), 2.31 (t, 2H × n, (−$OCOCH_2CH_2$−)$_n$), 3.28 (t, 2H, N_3CH_2−), 3.65 (t, 2H, −CH_2OH), 4.06 (t, 2H × n, (−CH_2CH_2O−)$_n$). ^{13}C NMR (150 MHz, $CDCl_3$, δ (ppm)): 24.5, 24.7, 25.0 ((−$CH_2CH_2CH_2$−)$_n$), 26.4, 28.9, 30.1 (−$CH_2CH_2CH_2$−), 31.9 (−CH_2CH_2OH), 33.9 (−$OCOCH_2$−), 51.3 (N_3CH_2−), 62.5 (−CH_2CH_2OH), 64.1 (−CH_2CH_2OCO−), 173.5 (−$OCOCH_2$−). The number-average molecular weight of the product was determined by calculated by proton ^{1}H NMR spectroscopy analysis: $\overline{M_{n,\,NMR}}$ = 11900 g/mol. The product was further characterized by using a gel permeation chromatography (GPC) system (Waters Alliance e2695 GPC system, Milford, MA, USA) equipped with Styragel® columns (HR1, HR2 and HR4), Waters 1515 isocratic pump and 2414 refractometer): PDI = 1.06. In the same manner, the other α-azido-ω-hydroxy-PCL precursors were prepared by the polymerizations with changing [M]/[I] ratio and time, followed by purifications and characterizations. The polymerization and characterization results are summarized in Table S1.

Table S1. Ring opening polymerization of ε-caprolactone (CL) using 6-azido-1-hexanol initiator and diphenyl phosphate catalyst in toluene [a]

Polymer	[M]/[I] [b]	Reaction time (h)	Yield [c] (%)	$M_{n,theo}$ [d] (g/mol)	$\overline{M_{n,NMR}}$ [e] (g/mol)	$\overline{M_{n,GPC}}$ [f] (g/mol)	PDI [g]
N_3-PCL_{30}-OH	30	5.0	97.3	3600	3940	4900	1.06
N_3-PCL_{70}-OH	70	10.0	96.5	8200	7850	10700	1.09
N_3-PCL_{100}-OH	100	20.0	96.4	11700	11900	16200	1.06
N_3-PCL_{150}-OH	150	29.0	97.3	17400	17200	20800	1.07
N_3-PCL_{200}-OH	200	42.0	97.1	23100	24300	26400	1.07

[a]Reaction temperature, 25 °C; [M], 1.0 mol/L. [b]Molar ratio of initial monomer and initiator. [c]Polymerization yield. [d]Molecular weight calculated from the conversion and the monomer to initiator ratio: [([M]/[I]) × conversion × (M_w of CL)] + (M_w of I). [e]Number-average molecular weight determined by ^{1}H NMR spectroscopy analysis. [f]Number-average molecular weight determined THF by using GPC analysis calibrated with polystyrene (PS) standards. [g]Polydispersity index determined by using GPC analysis calibrated with PS standards.

In the second-step, N_3-PCL_{100}-OH was further reacted with 5-hexynoic acid in CH_2Cl_2 at 25 °C under a nitrogen atmosphere by the aids of 1-ethyl-3-(3-dimethylaminopropyl)-carbodiimide (EDC) hydrochloride and 4-(dimethylamino)pyridine (DMAP). After 48 h, the reaction mixture was concentrated by using a rotary evaporator with a low vacuum system. The crude product was dissolved in CH_2Cl_2 and then precipitated into cold methanol several times to remove residual 5-hexynoic acid, EDC and DMAP, followed by filtration. The obtained product (N_3-PCL_{100}-C≡CH) was washed with cold methanol several times and dried at room temperature in vacuum. Yield: 96.8 %. $\overline{M_{n,NMR}}$ = 11900 g/mol; PDI = 1.10 (see the GPC trace in Fig. S1). ^{1}H NMR (300 MHz, $CDCl_3$, δ (ppm)): 1.38 (m, 2H × n, $(-CH_2CH_2CH_2CH_2CH_2-)_n$), 1.57 (m, 2H × n, $(-CH_2CH_2CH_2O-)_n$), 1.85 (quin, 2H, $-CH_2CH_2C\equiv C$), 1.98 (t, H, $-C\equiv CH$), 2.27 (m, 2H, $-CH_2C\equiv C$), 2.31 (t, 2H × n, $(-OCOCH_2CH_2-)_n$), 2.46 (t, 2H, $-CH_2CH_2CH_2C\equiv C$), 3.28 (t, 2H, N_3CH_2-), 4.06 (t, 2H × n, $(-CH_2CH_2O-)_n$). ^{13}C NMR (150 MHz, $CDCl_3$, δ (ppm)): 17.3 ($CH_2C\equiv CH$), 23.9, 24.5, 24.7, 25.0 ($(-CH_2CH_2CH_2-)_n$), 26.4, 28.9, 30.1 ($-CH_2CH_2CH_2-$), 31.9 ($-CH_2CH_2OH$), 32.7, 33.9 ($-OCOCH_2-$), 51.3 (N_3CH_2-), 64.2 ($-CH_2CH_2OCO-$), 69.0 ($-C\equiv CH$), 83.5 ($-CH_2CC\equiv H$), 173.4 ($-OCOCH_2-$).

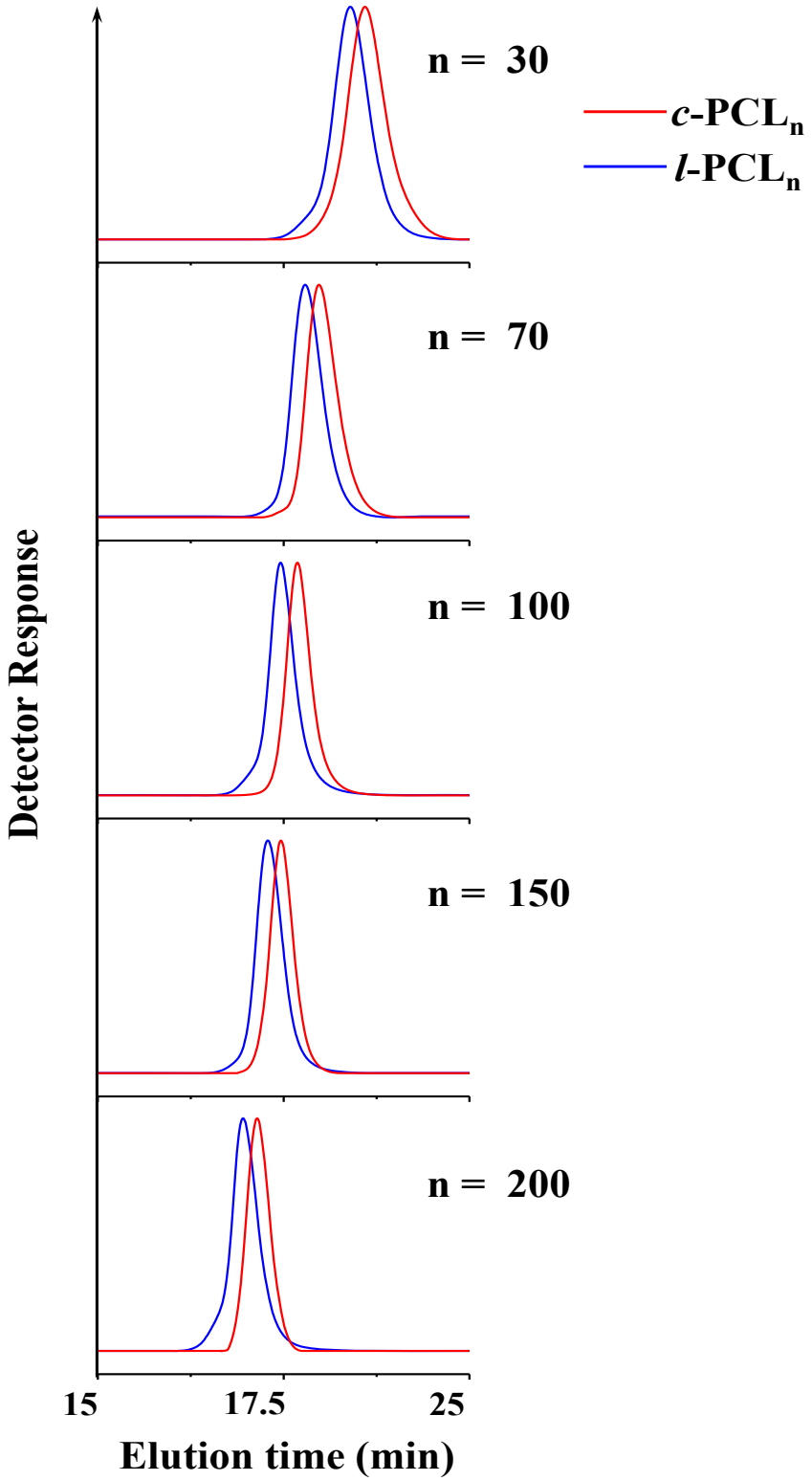

Fig. S1. Analytical GPC chromatograms: *l*-PCL$_n$ (N_3-PCL$_n$-C≡CH) precursors; *c*-PCL$_n$ products separated and fractionated (i.e., purified) by using preparative GPC (see Fig. S2).

In the same manner, the other α-azido-ω-ethynyl-PCLs were prepared, purified, and characterized. The ethynyl-capping esterification reaction and characterization results are summarized in Table S2.

Table 2. Ethynyl-capping esterification and characterization results of N_3-PCL$_n$-OH precursors

Polymer	Yield [a] (%)	$M_{n,theo}$ [b] (g/mol)	$\overline{M}_{n,NMR}$ [c] (g/mol)	$\overline{M}_{n,GPC}$ [d] (g/mol)	PDI [e]
N_3-PCL$_{30}$-C≡CH	97.7	3690	4000	5000	1.09
N_3-PCL$_{70}$-C≡CH	97.5	8300	7950	11100	1.08
N_3-PCL$_{100}$-C≡CH	96.8	11700	11900	16400	1.10
N_3-PCL$_{150}$-C≡CH	97.5	17500	17200	20800	1.11
N_3-PCL$_{200}$-C≡CH	97.6	23200	23200	26800	1.13

[a]Reaction yield. [b]Molecular weight estimated from the theoretical molecular weights of N_3-PCL$_n$-OH precursors in Table S1. [c]Number-average molecular weight determined by ^{1}H NMR spectroscopy analysis. [d]Number-average molecular weight determined THF by using GPC analysis calibrated with polystyrene (PS) standards. [e]Polydispersity index determined by using GPC analysis calibrated with PS standards.

In the third-step, the N_3-PCL$_{100}$-C≡CH (600 mg, 14.4 μmol) in degassed CH_2Cl_2 (36 mL) (0.00043 M precursor concentration) was added with a rate of 0.5 mL/h to a mixture of CuBr (395 86 mg, 0.976 mmol) and PMDETA (0.69 mL, 1.27 mmol) in degassed CH_2Cl_2 (350 mL) at 25 °C under flowing argon using a syringe pump (model Legato 100, KD Scientific, Holliston, MA, USA) equipped with a fine hypodermic needle (21 g × 30 cm). After the addition was completed, the reaction mixture was stirred for additional 3 h. Then, propargyl-functionalized polystyrene (PS-C≡CH) resin (3.0 g, 8.820 mmol) and a solution of CuBr (784 mg, 0.951 mmol) and PMDETA (1.38 mL, 1.24 mmol) were added in order to further reactions with unreacted precursor polymers as well as possibly formed linear dimers and multimers; here, PS-C≡CH resin was prepared by the treatment of 4-(hydroxymethyl)phenoxymethyl-polystyrene resin (polystyrene resin cross-linked with 1% divinylbenzene (200-400 mesh)) with propargyl bromide.[2,3] After stirred for 24 h, the reaction mixture was filtered, eliminated the unreacted precursors and possible linear dimers and mutlimers together with the used PS resin. The filtrate was concentrated by using a rotary evaporator. The crude product was

purified by using aluminum oxide columns (eluent, THF). The obtained product was further purified using a preparative GPC system, followed by drying at room temperature under vacuum. The recycling preparative GPC runs and fractionation were successfully carried out with THF (7.5mL/min) at 25 °C using a JAI GPC system (model LC-9260 II Next, Japan Analytical Industry, Tokyo, Japan) equipped with a JAI JAIGEL-2.5HH column (600 × 20.0 mm), a JAI JAIGEL-2HH column (600 × 20.0 mm) and a JAI RI-700 II NEXT refractive index detector, giving high purity target cyclic product (*c*-PCL_{100}) (Fig. S2 and Table S3). Here, it is noted that in this study the high performance separation and fractionation process using the recycling preparative GPC system, rather than simple precipitation methods, were conducted to get extremely high purity *c*-PCL product, even after the PS-C≡CH resin treatment to remove unreacted precursors and linear byproducts and subsequent filtration. The purified *c*-PCL products were further characterized by using an analytical GPC system calibrated with polystyrene standards (Fig. S1). Yield: 40.2%. The *c*-PCL_{100} product was additionally characterized by NMR spectroscopy. $\overline{M_{n,\,NMR}}$ = 12000 g/mol; PDI = 1.06. ^{1}H NMR (300 MHz, $CDCl_3$, δ (ppm)): 1.38(m, 2H × n, $(-CH_2CH_2CH_2CH_2CH_2-)_n$), 1.57(m, 2H × n, $(-CH_2CH_2CH_2O-)_n$), 2.31 (t, 2H × n, $(-OCOCH_2CH_2-)_n$), 2.76 (t, 2H, $-CH_2C{=}CH-$), 4.06(t, 2H × n, $(-CH_2CH_2O-)_n$), 4.43 (t, 2H, NCH_2-), 7.31 (s, 1H, triazole ring). ^{13}C NMR (150 MHz, $CDCl_3$, δ (ppm)): 24.4, 24.7, 25.1 ($(-CH_2CH_2CH_2-)_n$), 26.0, 26.4, 29.9, 30.1, ($-CH_2CH_2CH_2-$), 33.6 ($-OCOCH_2-$), 57.0 ($-CH_2CH_2N-$), 66.7 ($-CH_2CH_2OCO-$), 120.2 (triazole ring), 146.8 (triazole ring), 173.5($-OCOCH_2-$). The *c*-PCL_{100} product was further confirmed by using an infrared (IR) spectrometer (model Research Series 2, ATI Mattson, Madison, WI, USA) equipped with a liquid nitrogen-cooled mercury cadmium telluride (MCT) detector (Fig. S3). In the same manner, cyclization reactions were conducted for the other α-azido-ω-ethynyl-PCLs, then followed by purifications and characterizations. The azide-ethyne cyclization reaction and characterization results are summarized in Table S4.

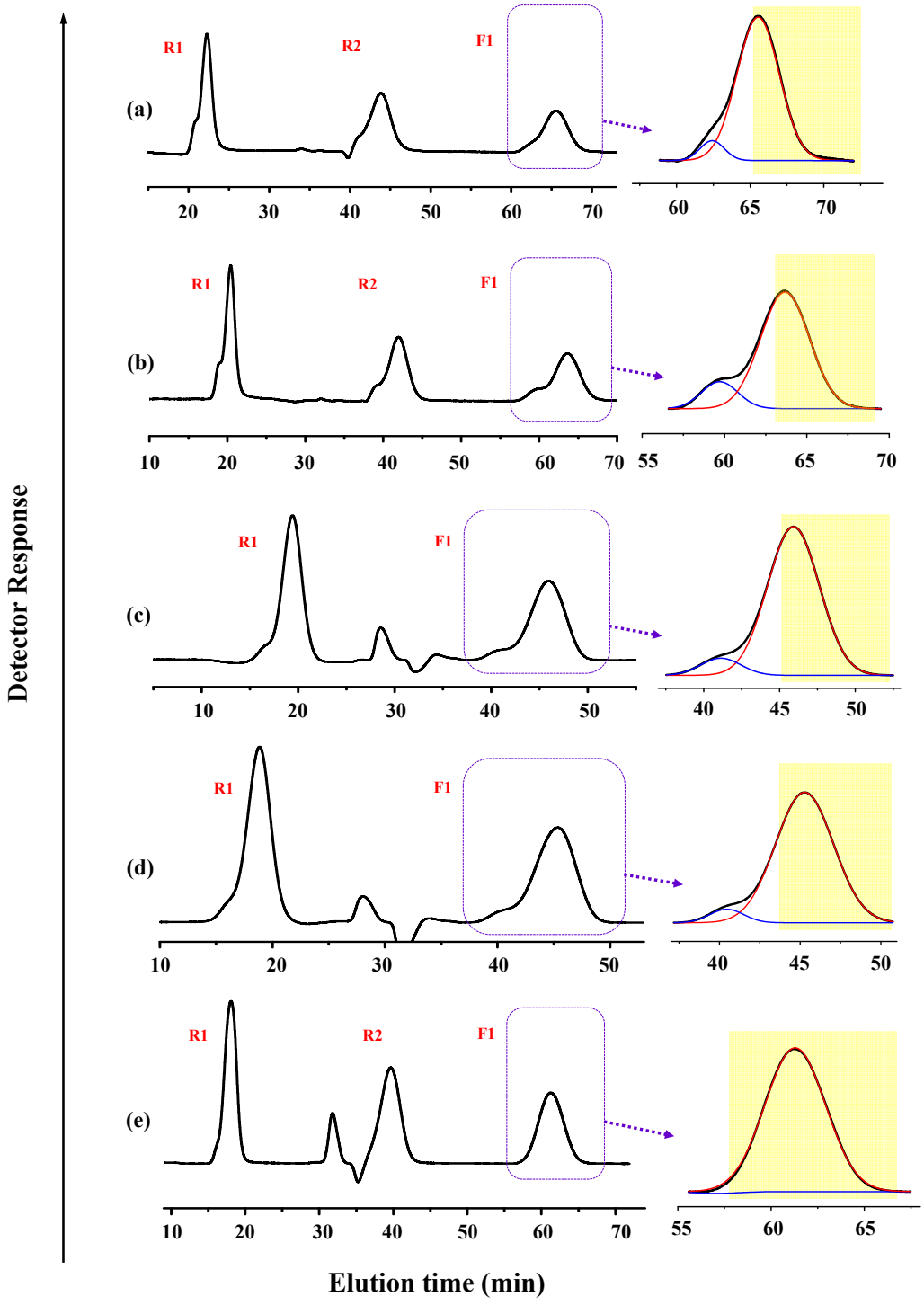

Fig. S2. Purification (i.e., separation and fractionation) of *c*-PCL$_n$ from the cyclization reaction medium using a recycling preparative GPC system, after PS-C≡CH) resin treatment and subsequent filtration (i.e., removal of unreacted precursor polymers and possibly formed linear dimers and multimers) and additional purification with aluminum oxide columns (i.e., removal of the used catalyst and PMDETA): : (a) *c*-PCL$_{30}$; (b) *c*-PCL$_{70}$; (c) *c*-PCL$_{100}$; (d) *c*-PCL$_{150}$; (e) *c*-PCL$_{200}$. **R1** and **R2** indicate the first and second cycling runs respectively in the GPC operation. **F1** means the fractionation of *c*-PCL product; the *c*-PCL product marked with yellow color was fractionated.

Table S3. Preparative GPC-based separation and fractionation results of the reaction mixtures obtained by click cyclization reactions of N_3-PCL_n-C≡CH (*l*-PCL_n) precursors

Precursor reactant	Reaction mixture[a]		
	c-PCL[b] (%)	Cyclic byproducts[c] (%)	Linear polymers[d] (%)
l-PCL_{30}	38.1	3.8	58.1
l-PCL_{70}	39.5	8.3	52.2
l-PCL_{100}	40.2	4.0	55.8
l-PCL_{150}	40.5	2.6	56.9
l-PCL_{200}	41.1	0.4	58.5

[a]Reaction mixture obtained by click cyclization reaction. [b]Cyclic PCL obtained by the separation and fractionation using a preparative GPC system after treated with PS-C≡CH resins. [c]Cyclic byproducts obtained by the separation and fractionation using a preparative GPC system after treated with PS-C≡CH resins. [d]Sum of the unreacted precursor polymers and possible linear byproducts removed by treatment with PS-C≡CH resins; this was estimated from the yield of cyclic PCL product and the preparative GPC analysis result.

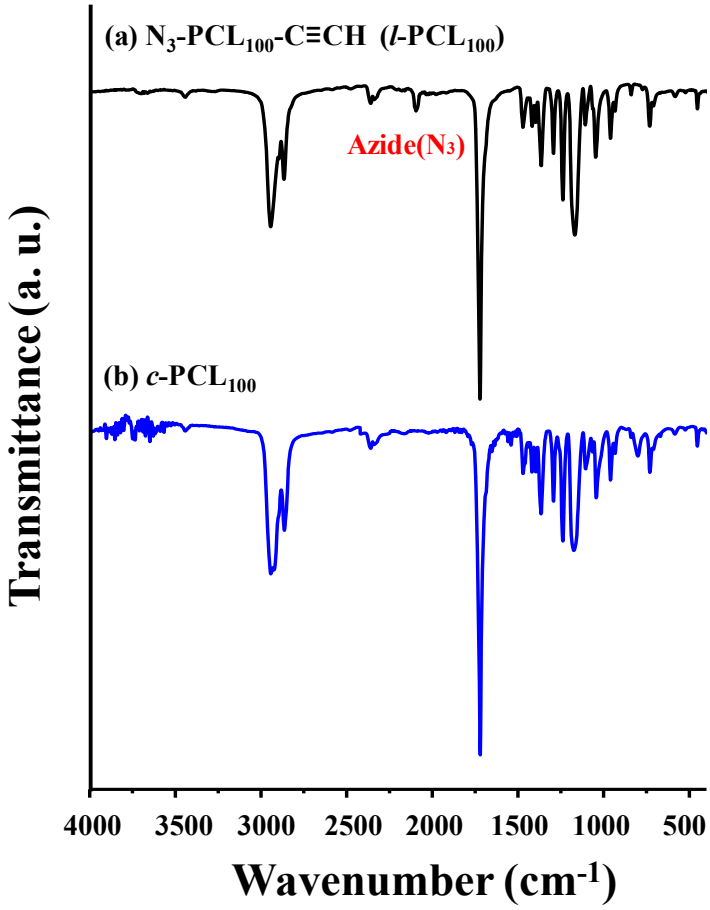

Fig. S3. FT-IR spectra of N_3-PCL_{100}-C≡CH (*l*-PCL_{100}) and its cyclization product (*c*-PCL_{100}).

Table S4. Azide-ethyne cyclization and characterization results of N_3-PCL_n-C≡CH precursors

Polymer	Yield [a] (%)	$M_{n,theo}$ [b] (g/mol)	$\overline{M}_{n,NMR}$ [c] (g/mol)	$\overline{M}_{n,GPC}$ [d] (g/mol)	PDI [e]
c-PCL_{30}	38.1	3700	4100	3700	1.09
c-PCL_{70}	39.5	8300	8000	7900	1.10
c-PCL_{100}	40.2	11800	12000	12100	1.06
c-PCL_{150}	40.5	17500	17300	15300	1.13
c-PCL_{200}	41.1	23300	23200	21500	1.11

[a]Reaction yield. [b]Molecular weight estimated from the theoretical molecular weights of N_3-PCL_n-C≡CH precursors in Table S2. [c]Number-average molecular weight determined by ^{1}H NMR spectroscopy analysis. [d]Number-average molecular weight determined THF by using GPC analysis calibrated with polystyrene (PS) standards. [e]Polydispersity index determined by using GPC analysis calibrated with PS standards.

The obtained *c*-PCL_n products and their linear counterparts were examined by differential scanning calorimetry (DSC). Representatives and analysis results of the measured DSC thermograms are presented in Fig. S4 and Table S5, respectively.

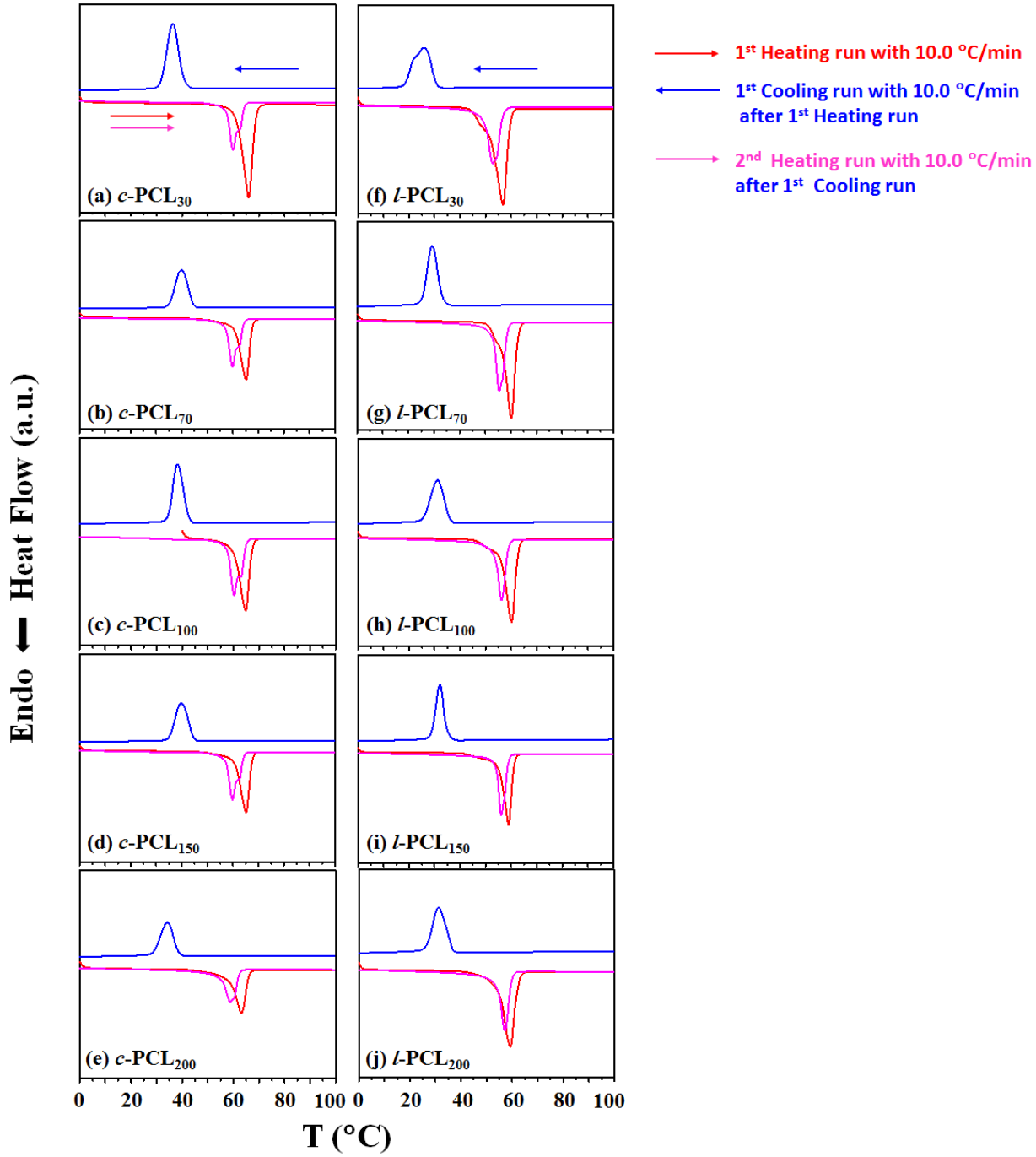

Fig. S4. DSC thermograms of the as-synthesized *c*-PCL_n and *l*-PCL_n (N_3-PCL_n-C≡CH) products in bulk states, which were measured with a rate of 10.0 °C/min by sequential runs: 1st heating run and subsequent cooling run from the melt and reheating run.

Table S5. Thermal transition characteristics of *c*-PCL_n and *l*-PCL_n products

Polymer	1st Heating run[a]		1st Cooling run[b]		2nd Heating run[c]	
	T_m [d] (°C)	ΔH_m [e] (J/g)	T_c [f] (°C)	ΔH_m [g] (J/g)	T_m [h] (°C)	ΔH_m [i] (J/g)
c-PCL_{30}	66.0	145.9	37.6	-117.8	61.8	121.9
c-PCL_{70}	65.2	81.72	38.3	-60.28	61.3	70.06
c-PCL_{100}	64.8	93.4	38.2	-81.77	61.2	97.12
c-PCL_{150}	65.2	88.61	37.5	-75.54	60.9	85.12
c-PCL_{200}	63.1	72.92	38.6	-58.92	61.6	70.99
l-PCL_{30}	56.8	162.1	33.5	-91.35	55.5	106.20
l-PCL_{70}	60.2	132.4	32.5	-84.10	55.6	95.95
l-PCL_{100}	60.1	124.9	32.8	-77.31	56.4	90.74
l-PCL_{150}	59.0	95.04	32.5	-63.68	56.1	71.86
l-PCL_{200}	59.3	127.0	31.8	-81.17	56.2	95.57

[a] 1st Heating run of the as-synthesized polymer sample in DSC analysis (Fig. S4). [b] 1st Cooling run of the as-synthesized polymer sample after the 1st heating run in DSC analysis (Fig. S4). [c] 2nd Heating run of the as-synthesized polymer sample after the 1st cooling run from the melt in DSC analysis (Fig. S4). [d] Temperature at the peak maximum of the crystal melting transition in the 1st Heating run with a heating rate of 10.0 °C/min. [e] Heat of fusion for crystal melting in the 1st Heating run with a rate of 10.0 °C/min. [f] Crystallization temperature at the peak maximum of the crystallization transition in the 1st Cooling run with 10.0 °C/min from the melt after the 1st Heating run. [g] Heat of fusion for crystallization in the 1st Cooling run with 10.0 °C/min from the melt after the 1st Heating run. [h] Temperature at the peak maximum of the crystal melting transition in the 2nd Heating run with 10.0 °C/min after the 1st Cooling run with 10.0 °C/min from the melt. [i] Heat of fusion for crystal melting in the 2nd Heating run with 10.0 °C/min after the 1st Cooling run with 10.0 °C/min from the melt.

GIXS Data Analysis

The intensity of GIXS (I_{GIXS}) from structures in a thin film can be expressed by the scattering formula:[4-7]

$$I_{\mathrm{GIXS}}(\alpha_{\mathrm{f}}, 2\theta_{\mathrm{f}}) \cong \frac{1}{16\pi^2} \cdot \frac{1-e^{-2\mathrm{Im}(q_z)t}}{2\mathrm{Im}(q_z)} \cdot \begin{bmatrix} |T_{\mathrm{i}}T_{\mathrm{f}}|^2 I_1\left(q_{\parallel}, \mathrm{Re}(q_{1,z})\right) + \\ |T_{\mathrm{i}}T_{\mathrm{f}}|^2 I_1\left(q_{\parallel}, \mathrm{Re}(q_{2,z})\right) + \\ |T_{\mathrm{f}}T_{\mathrm{i}}|^2 I_1\left(q_{\parallel}, \mathrm{Re}(q_{3,z})\right) + \\ |T_{\mathrm{i}}T_{\mathrm{f}}|^2 I_1\left(q_{\parallel}, \mathrm{Re}(q_{4,z})\right) \end{bmatrix} \quad (1)$$

where α_{f} and $2\theta_{\mathrm{f}}$ are the out-of-plane and in-plane exit angle of the out-going X-ray beam respectively, $\mathrm{Im}(q_z) = |\mathrm{Im}(k_{z,f})| + |\mathrm{Im}(k_{z,i})|$, $\mathrm{Re}(x)$ is the real part of x, t is the film thickness, R_i and T_i are the reflected and transmitted amplitudes of the incoming X-ray beam respectively, and R_f and T_f are the reflected and transmitted amplitudes of the outgoing X-ray beam respectively. In addition, $q_{\parallel} = \sqrt{q_x^2 + q_y^2}$, $q_{1,z} = k_{z,f} - k_{z,i}$, $q_{2,z} = -k_{z,f} - k_{z,i}$, $q_{3,z} =$

$k_{z,f} + k_{z,i}$, and $q_{4,z} = -k_{z,f} + k_{z,i}$; here, $k_{z,i}$ is the z-component of the wave vector of the incoming X-ray beam, which is given by $k_{z,i} = k_0\sqrt{n_R^2 - \cos^2\alpha_i}$, and $k_{z,f}$is the z-component of the wave vector of the outgoing X-ray beam, which is given by $k_{z,f} = k_0\sqrt{n_R^2 - \cos^2\alpha_f}$, where $k_0 = 2\pi/\lambda$, λ is the wavelength of the X-ray beam, n_R is the refractive index of the film given by $n_R = 1 - \delta + i\zeta$ with dispersion δ and absorption ζ, and α_i is the out-of-plane grazing incident angle of the incoming X-ray beam. q_x, q_y, and q_z are the components of the scattering vector **q**. I_1 is the scattering intensity of the structure in the film, which can be calculated kinematically.

In eq (1), I_1 is the scattered intensity from morphological structures in the film and, thus, can be expressed by the following equation:[4-9]

$$I_1(\mathbf{q}) = P(\mathbf{q}) \cdot S(\mathbf{q}) \tag{2}$$

where $P(\mathbf{q})$ is the form factor that describes the shape, size, and orientation of scatterers in a thin film, and $S(\mathbf{q})$ is the structure factor which provides information on the relative positions of the group of scatterers, such as the crystal lattice parameters, orientation, dimension, and symmetry in an ordered structure and the interdistance of domains.

The measured grzazing incidence small angle X-ray scattering (GISAXS) patterns inform that horizontally-oriented lamellar structures were formed in ca. 40 nm thick PCL films. To analyze the GISAXS data, those lamellar structures may be appropriately handled by using a three layer model that is composed of a dense layer, a less dense layer, and their interfacial layer (Figure S3). For the lamellar structure consisted of three layers, the form factor $P(\mathbf{q})$ can be expressed by the following equation:[10]

$$P(\mathbf{q}) = \left[\begin{array}{l} 4L_xL_yH_{in}(\rho_{in} - \rho_{ex}) \cdot \frac{\sin(q_xL_x)}{q_xL_x} \cdot \frac{\sin(q_yL_y)}{q_yL_y} \cdot \frac{\sin(q_zH_{in})}{q_zH_{in}} + \\ 4L_xL_yH_{ex}(\rho_{ex} - \rho_{matrix}) \cdot \frac{\sin(q_xL_x)}{q_xL_x} \cdot \frac{\sin(q_yL_y)}{q_yL_y} \cdot \frac{\sin(q_zH_{ex})}{q_zH_{ex}} \end{array} \right]^2 \tag{3}$$

where L_x and L_y are the length and width of lamellar structure respectively, H_{in} and H_{ex} are the interior and exterior layer heights, respectively, and ρ_{in} and ρ_{ex} are the corresponding

relative electron densities. ρ_{matrix} is the relative electron density of the matrix layer. Considering the electron density contrast in lamellar structure formed in the PCL thin films, H_{in} corresponds to the dense thickness (= l_1) having a relatively electron density ρ_{in}. The exterior layer thickness having a relatively electron density $\rho_{exterior}$ corresponds to the interfacial layer and is estimated from H_{in} and H_{ex}: $l_2 = (H_{ex} - H_{in})/2$. The matrix layer corresponds the sparse layer with thickness l_3 and the relatively electron density ρ_{matrix} is obtained from the long period L that is extracted from the structure factor $S(\mathbf{q})$: $l_3 = (L - l_1 - 2l_2)$. For the lamellar structures formed in the PCL thin films, dense layer (H_{in} and l_1) corresponds to the highly dense crystalline layer, and the interfacial layer (H_{ex} and l_2) corresponds to the less dense crystalline layer, and the sparse dense layer (l_3) the amorphous layer of PCL.

For the above form factor, structural parameter is further assumed to follow a Gaussian distribution $G(A)$:

$$G(A) = \frac{1}{\sqrt{2\pi}\sigma_A} exp\left[-\frac{(A-\bar{A})^2}{2\sigma_A^2}\right] \quad (4)$$

where A can be one of the parameters, A is the mean value, and $\bar{A}$ is the standard deviation of A from $\bar{A}$.

A paracrystal model is most appropriate using as the structural factor model. For a paracrystalline lattice consisting of the three layers described above, the structure factor S(q) (the so-called interference function or lattice factor) can be determined from the Fourier transform of a complete set of lattice points.[7-10] In a paracrystal with distortion of the second kind, the positions of the lattice points can only be described with a positional distribution function (i.e., g-factor). In the simple case where the autocorrelation function of the crystal lattice is given by the convolution product of the distributions of the lattice points along three axes, and the distribution function is a Gaussian, S(q) can be expressed by the following equation:

$$S(\mathbf{q}) = \prod_{k=1}^{3} Z_k(\mathbf{q}) \quad (5)$$

$$Z_k(\mathbf{q}) = 1 + \frac{F_k(\mathbf{q})}{1-F_k(\mathbf{q})} + \frac{F_k^*(\mathbf{q})}{1-F_k^*(\mathbf{q})} \quad (6)$$

$$F_k(\mathbf{q}) = |F_k(\mathbf{q})|e^{-iqa_k} \tag{7}$$

$$|F_k(\mathbf{q})| = exp\left[-\frac{1}{2}(q_1^2 g_1^2 + q_2^2 g_2^2 + q_3^2 g_3^2)\right] \tag{8}$$

Here g_1, g_2, and g_3 are the components of the *g*-factor defined as

$$g_1 = \Delta\mathbf{a_1}/\mathbf{a_1} \tag{9a}$$

$$g_2 = \Delta\mathbf{a_2}/\mathbf{a_2} \tag{9b}$$

$$g_3 = \Delta\mathbf{a_3}/\mathbf{a_3} \tag{9c}$$

where $\mathbf{a_k}$ is the component of the fundamental vector a of the domain structure and $\Delta\mathbf{a_k}$ is the displacement of the vector $\Delta\mathbf{a_k}$. And q_1, q_2, and q_3 are the components of the scattering vector $\mathbf{q}$.

For the lamellar structure composed of three layers (Figure S11), the components of $\mathbf{q}$ in eq (8) are defined by

$$q_1 = \mathbf{a_1} \cdot \mathbf{q_x} = |d_x \times \mathbf{q_x}| \tag{10a}$$

$$q_2 = \mathbf{a_2} \cdot \mathbf{q_y} = |d_y \times \mathbf{q_y}| \tag{10b}$$

$$q_3 = \mathbf{a_3} \cdot \mathbf{q_z} = |L \times \mathbf{q_z}| \tag{10c}$$

where d_x and d_y are the lattice dimension parameters (i.e., d-spacing values) along the q_x- and q_y direction, respectively, and L is the long period along the q_z-direction.

Moreover, for a structure with a given orientation in a film, its fundamental vectors can be rotated and transformed by a rotation matrix. When the structure of the film is randomly oriented in the plane of the film but uniaxially oriented out of plane, the peak position vector qc of a certain reciprocal lattice point c* in the sample reciprocal lattice is given by

$$\mathbf{q_c} = \mathbf{R} \cdot \mathbf{c}^* \equiv (q_{c,x}, q_{c,y}, q_{c,z}) \tag{11}$$

where $\mathbf{R}$ is a 3×3 matrix to decide the preferred orientation of the structure in the film, and

$q_{c,x}$, $q_{c,y}$, and $q_{c,z}$ are the x, y, z components of the peak position vector $\mathbf{q_c}$, respectively. Using eq (11), every peak position can be obtained. Because of cylindrical symmetry, the Debye-Scherrer ring composed of the in-plane randomly oriented c* cuts an Ewald sphere at two positions in its top hemisphere: $q_{\parallel} = q_{c,\parallel} \equiv \pm\sqrt{q_{c,x}^2 + q_{c,y}^2}$ with $q_z = q_{c,z}$. Thus diffraction patterns with cylindrical symmetry are easily calculated in the q-space. It is then convenient to determine the preferred orientation of known structures and further to analyze anisotropic X-ray scattering patterns. However, since **q**-space is distorted in GIXS by refraction and reflection effects, the relation between the detector plane expressed as the Cartesian coordinate defined by two perpendicular axes (i.e., by $2\theta_f$ and α_f) and the reciprocal lattice points is needed. The two wave vectors $k_{z,i}$ and $k_{z,f}$ are corrected for refraction as $k_{z,i} = k_o\sqrt{n_R^2 - \cos^2\alpha_i}$ and $k_{z,f} = k_o\sqrt{n_R^2 - \cos^2\alpha_f}$, respectively. Therefore, the two sets of diffractions that result from the incoming and outgoing X-ray beams, and denoted by q_1 and q_3 respectively, are given at the exit angles by the following expression:

$$\alpha_f = \arccos\left(\sqrt{n_R^2 - \left(\frac{q_{c,z}}{k_o} \pm \sqrt{n_R^2 - \cos^2\alpha_i}\right)^2}\right) \tag{12}$$

where $q_{c,z}/k_o > \sqrt{n_R^2 - \cos^2\alpha_i}$. In eq (11), the positive sign denotes diffractions produced by the outgoing X-ray beam, and the negative sign denotes diffractions produced by the incoming X-ray beam. The in-plane incidence angle $2\theta_i$ is usually zero, so the in-plane exit angle $2\theta_f$ can be expressed as follows.

$$2\theta_f = arccos\left[\frac{\cos^2\alpha_i + \cos^2\alpha_f - \left(\frac{q_{c,\parallel}}{k_o}\right)^2}{2\ \cos\alpha_i\ \cos\alpha_f}\right]. \tag{13}$$

Therefore, diffraction spots detected on the detector plane in GIXS measurements can be directly compared to those derived using eqs (11)-(13) from an appropriate model and thus analyzed in terms of the model.

To obtain information on the orientation of the paracrystal lattice of the phase separated micro domain structures from GIXS data, the distribution of the orientation vector $\mathbf{n_i}$ is given by a function $D(\varphi)$, where φ is the polar angle between the $\mathbf{n_i}$ vector and the out-of-plane of

the film (see Fig. S7); for example, φ is zero when the $\mathbf{n_i}$ vector in the film is oriented normal to the film plane. To calculate the 2D GIXS patterns, $D(\varphi)$ should be represented by a numerical function. In relation to the distribution of the lattice orientation, $D(\varphi)$can generally be considered as a Gaussian distribution:

$$D(\varphi) = \frac{1}{\sqrt{2\pi}\sigma_\varphi} \exp\left[-\frac{(\varphi-\bar{\varphi})^2}{2\sigma_\varphi^2}\right] \quad (14)$$

where $\bar{\varphi}$ and σ_φ are the mean angle and standard deviation of φ from $\bar{\varphi}$, respectively. The observed scattering intensity $I_{\mathrm{GIXS},\varphi}(\mathbf{q})$ is obtained by integrating $I_{\mathrm{GIXS},\varphi}(\mathbf{q})$ over possible orientations of the lattice:

$$I_{\mathrm{GIXS},\varphi}(\mathbf{q}) = \int_{-\pi}^{\pi} I_{\mathrm{GIXS}}(\mathbf{q}) D(\varphi) d\varphi. \quad (15)$$

The second order orientation factor O_s can be defined as the following equation:[11-13]

$$O_s = \int D(\varphi) \frac{(3\cos^2\varphi - 1)}{2} d\varphi \quad (16)$$

When $D(\varphi)$ is strongly peaked around φ= 0° (i.e. vertical alignment), cosφ= 1 and O_s = 1. On the other hand, when φ = 90°, cosφ= 0 and O_s = -0.5. If the orientation is entirely random, $\langle\cos^2\varphi\rangle$ = 1/3 and O_s = 0. Thus, O_s is a measure of the orientation of nanostructures.

References

1 L. Xiang, W. Ryu, H. Kim and M. Ree, *Polymers*, 2018, **10**, 577.

2 J. Rao, J. Zhang and S. Liu, *Biomacromolecules*, 2008, **9**, 2586.

3 C. N. Urbani, C. Bell, D. Lonsdale, M. R. Whittaker and M. J. Monteiro, *Macromolecules*, 2007, **40**, 7056.

4 (a) B. Lee, I. Park, J. Yoon, S. Park, J. Kim, K.-W. Kim, T. Chang and M. Ree, *Macromolecules*, 2005, **38**, 4311. (b) M. Ree, *Macromol. Rapid Commun.* 2014, **35**, 930.

5 (a) J. Yoon, S. Y. Yang, K. Heo, B. Lee, W. Joo, J. K. Kim and M. Ree, *J. Appl.*

Crystalogr., 2007, **40**, 305. (b) J. Yoon, S. Jin, B. Ahn, Y. Rho, T. Hirai, R. Maeda, T. Hayakawa, J. Kim, K.-W. Kim and M. Ree, *Macromolecules*, 2008, **41**, 8778.

6 (a) B. Lee, Y.-H. Park, Y. Hwang, W. Oh, J. Yoon and M. Ree, *Nat. Mater.*, 2005, **4**, 147. (b) B. Lee, W. Oh, Y. Hwang, Y.-H. Park, J. Yoon, K. S. Jin, K. Heo, J. Kim, K.-W. Kim and M. Ree, *Adv. Mater.*, 2005, **17**, 696. (c) B. Lee, J. Yoon, W. Oh, Y. Hwang, K. Heo, K. S. Jin, J. Kim, K.-W. Kim and M. Ree, *Macromolecules*, 2005, **39**, 3395.

7 K. Heo, K. S. Jin, J. Yoon, S. Jin, W. Oh and M. Ree, *J. Phys. Chem. B*, 2006, **110**, 15887.

8 (a) Y. J. Roe, Methods of X-ray and Neutron Scattering in Polymer Science. New York: Oxford University Press; 2000. (b) R. Lazzari, *J. Appl. Crystallogr.*, 2002, **35**, 406. (c) G. Renaud, R. Lazzari and F. Leroy, *Surf. Sci. Rep.*, 2009, **64**, 255.

9 (a) J. S. Pedersen, *J. Appl. Crystallogr.*, 1994, **27**, 595. (b) R. Hosemann, S. N. Bagchi, Direct analysis of diffraction by matter. Amsterdam: North-Holland; 1962.

10 (a) Y. Y. Kim, B. J. Ree, M. Kido, Y. Ko, R. Ishige, T. Hirai, D. Wi, J. Kim, W. J. Kim, A. Takahara and M. Ree, *Adv. Electron. Mater.*, 2005, **1**, 1500197. (b) R. Phinjaroenphan, Y. Y. Kim, B. J. Ree, T. Isono, J. Lee, S. Rugmai, H. Kim, S. Maensiri, T. Kakuchi, T. Satoh and M. Ree, *Macromolecules*, 2015, **48**, 5816.

11 Y. Rho, J. Min, J. Yoon, B. Ahn, S. Jung, K. Kim, P. Shah, J.-S. Lee and M. Ree, *NPG Asia Mater.*, 2012, **4**, e29.

12 (a) B. Ahn, D. M. Kim, J.-C. Hsu, Y.-G. Ko, T. J. Shin, J. Kim, W.-C. Chen and M. Ree, *ACS Macro Letters*, 2013, **2**, 555. (b) S. G. Hahm, Y. Rho, J. Jung, S. H. Kim, T. Sajoto, F. S. Kim, S. Barlow, C. E. Park, S. A. Jenekhe, S. R. Marder and M. Ree, *Adv. Funct. Mater.*, 2013, **23**, 2060.

13 M. Matsuo, M. Tamada, T. Terada, C. Sawatari and M. Niwa, *Macromolecules*, 1982, **15**, 988.

Table S6. Morphological structure parameters of nanoscale films of *c*-PCL$_n$ polymers and linear counterparts obtained by synchrotron XR analysis

Structural parameter	Nanoscale film				
	***c*-PCL$_{30}$**	***c*-PCL$_{70}$**	***c*-PCL$_{100}$**	***c*-PCL$_{150}$**	***c*-PCL$_{200}$**
ρ_e [a] (e's/nm^3)	395 (3) [e]	379 (3)	358 (3)	353 (3)	351 (3)
ρ_m [b] (g/cm^3)	1.21 (0.01)	1.16 (0.01)	1.10 (0.01)	1.08 (0.01)	1.07 (0.01)
t_f [c] (nm)	31.1 (0.1)	35.3 (0.1)	34.2 (0.1)	34.8 (0.1)	41.1 (0.1)
σ_f [d] (nm)	1.1 (0.1)	1.9 (0.1)	2.1 (0.1)	1.9 (0.1)	2.4 (0.1)
	***l*-PCL$_{30}$**	***l*-PCL$_{70}$**	***l*-PCL$_{100}$**	***l*-PCL$_{150}$**	***l*-PCL$_{200}$**
ρ_e (e's/nm^3)	364 (3)	354 (3)	337 (3)	335 (3)	337 (3)
ρ_m (g/cm^3)	1.11 (0.01)	1.08 (0.01)	1.03 (0.01)	1.02 (0.01)	1.03 (0.01)
t_f (nm)	34.3 (0.1)	34.3 (0.1)	46.1 (0.1)	35.9 (0.1)	39.7 (0.1)
σ_f (nm)	2.0 (0.1)	2.0 (0.1)	2.0 (0.1)	2.0 (0.1)	2.1 (0.1)

[a]Electron density. [b]Mass density estimated from the measured electron density. [c]Film thickness. [d]Film surface roughness. [e]Standard deviation.

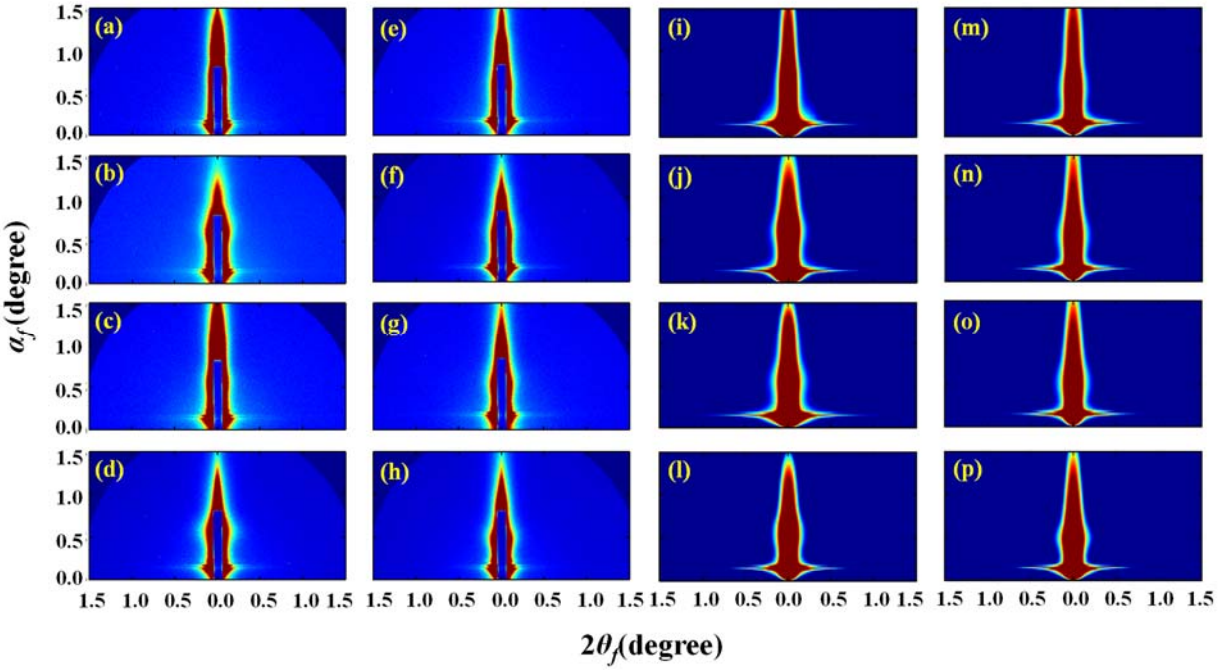

Fig. S5. 2D GISAXS images of nanoscale films of *c*-PCL$_n$ and linear counterparts at room temperature: (a) *c*-PCL$_{30}$ (α_i = 0.146°); (b) *c*-PCL$_{70}$ (α_i = 0.150°); (c) *c*-PCL$_{100}$ (α_i = 0.144°); (d) *c*-PCL$_{150}$ (α_i = 0.150°); (e) *l*-PCL$_{30}$ (α_i = 0.152°); (f) *l*-PCL$_{70}$ (α_i = 0.151°); (g) *l*-PCL$_{100}$ (α_i = 0.152°); (h) *l*-PCL$_{150}$ (α_i = 0.151°). Reconstructed 2D GISAXS images: (i) *c*-PCL$_{30}$; (j) *c*-PCL$_{70}$; (k) *c*-PCL$_{100}$; (l) *c*-PCL$_{150}$; (m) *l*-PCL$_{30}$; (n) *l*-PCL$_{70}$; (o) *l*-PCL$_{100}$; (p) *l*-PCL$_{150}$. The scattering measurements were conducted with an X-ray beam of λ = 0.1278 nm (wavelength) at room temperature.

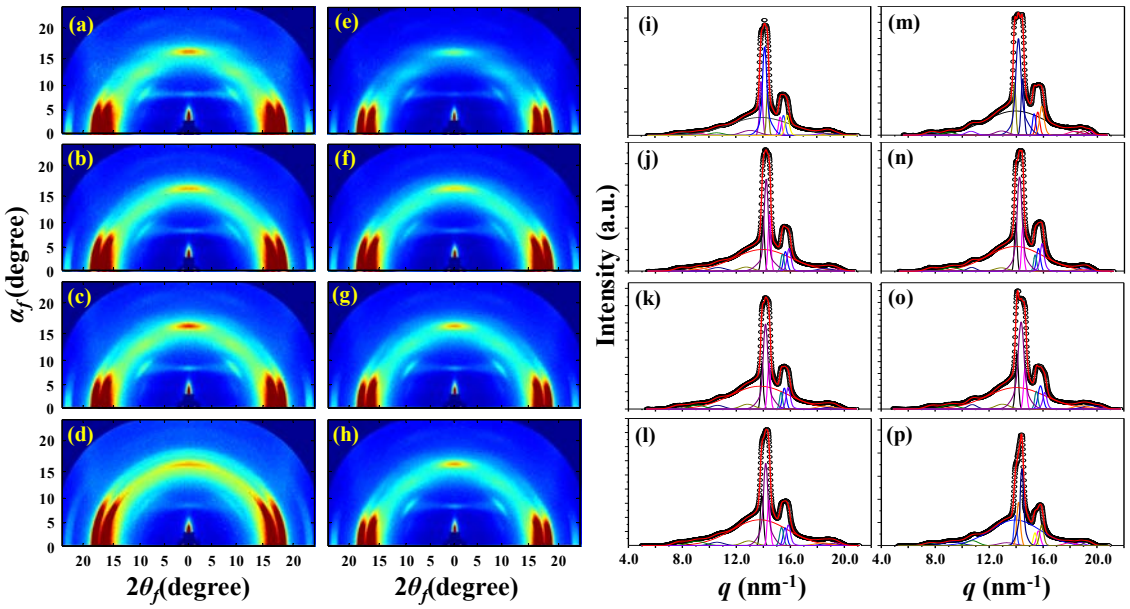

Fig. S6. GIWAXS analysis of nanoscale films of *c*-PCL$_n$ and linear counterparts at room temperature; 2D GIWAXS images: (a) *c*-PCL$_{30}$ (α_i = 0.187°, grazing incidence angle); (b) *c*-PCL$_{70}$ (α_i = 0.176°); (c) *c*-PCL$_{100}$ (α_i = 0.187°); (d) *c*-PCL$_{150}$ (α_i = 0.176°); (e) *l*-PCL$_{30}$ (α_i = 0.197°); (f) *l*-PCL$_{70}$ (α_i = 0.187°); (g) *l*-PCL$_{100}$ (α_i = 0.197°); (h) *l*-PCL$_{150}$ (α_i = 0.186°); quadrant-averaged scattering profiles obtained from the images in (a-h): (i) *c*-PCL$_{30}$; (j) *c*-PCL$_{70}$; (k) *c*-PCL$_{100}$; (l) *c*-PCL$_{150}$; (m) *l*-PCL$_{30}$; (n) *l*-PCL$_{70}$; (o) *l*-PCL$_{100}$; (p) *l*-PCL$_{150}$. In (i-p), the symbols represent the measured data and the red line is the sum of the amorphous phase peak (dark orange line) and crystalline peaks (all other colored lines) separated by using the Peakfit® software. The scattering measurements were conducted with an X-ray beam of λ = 0.1278 nm (wavelength) at room temperature.

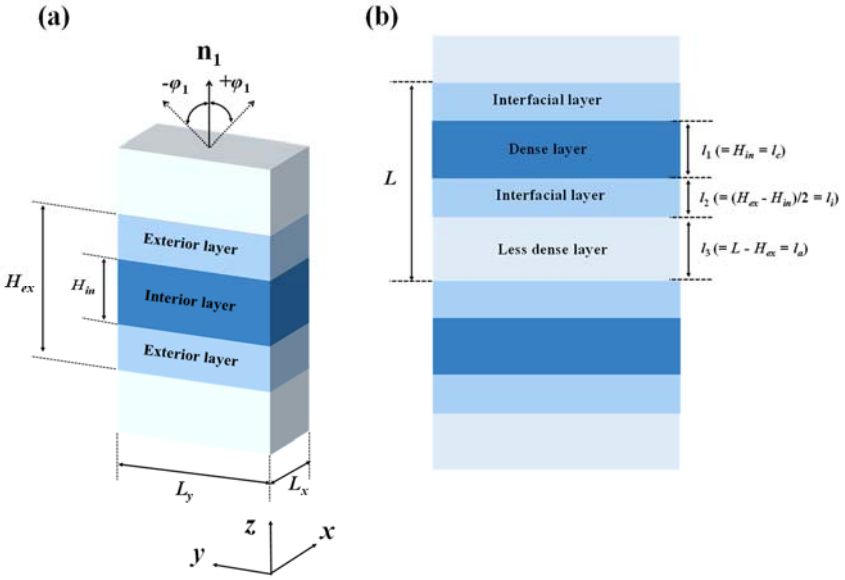

Fig. S7. A lamellar structure model composed of three layers: (a) 3D representation of lamellar structure where $\mathbf{n}_1$ is the orientation vector of the structure and φ_1 is the polar angle between the $\mathbf{n}_1$ vector and the out-of-plane of the film; (b) 2D representation of lamellar structure. The interior and exterior layers in (a) correspond to the dense (i.e., crystalline layer) and interfacial layers in (b) respectively; the lightest blue colored layer in (b) corresponds to the less dense layer (i.e., amorphous layer). The dimension of the lamellar structure is defined by L (long period), L_x, L_y, l_1 (= H_{in} = l_c), l_2 (= (H_{ex} – H_{in})/2 = l_i), and l_3 (= L – H_{ex} = l_a).